Annals of Nuclear Energy 166 (2022) 108830

Contents lists available at ScienceDirect

Annals of Nuclear Energy

journal homepage: www.elsevier.com/locate/anucene

Design of Cesium target assembly with YH_2 moderator and Gd thermal neutron shielding to produce ^{135}Cs for LLFP transmutation study using the experimental fast reactor Joyo

Yoshihisa Tahara [a,1], Peng Hong Liem [a,b,*], Naoyuki Takaki [a], Satoshi Chiba [c]

[a] Tokyo City University, 1-28-1, Tamazutsumi, Setagaya, Tokyo 158-8557, Japan
[b] Nippon Advanced Information Service (NAIS Co., Inc.), 416 Muramatsu, Tokaimura, Ibaraki 319-1112, Japan
[c] Tokyo Institute of Technology, 2-12-1 N1-12, Ookayama, Meguro, Tokyo 152-850, Japan

ARTICLE INFO

Article history:
Received 2 November 2020
Received in revised form 6 November 2021
Accepted 9 November 2021

Keywords:
LLFP
^{135}Cs
Fast reactor
Joyo
Hydride
Gadolinium
Irradiation

ABSTRACT

In this design study, we investigated the feasibility of producing a sufficient amount of ^{135}Cs long-lived fission product (LLFP) in the Joyo fast reactor by irradiation of natural cesium (^{133}Cs). The irradiation is expected to contribute to providing ^{135}Cs sample for transmutation cross-section measurements for enhancing the accuracy of the LLFP nuclear data. Two irradiation fields, one located in the outer reflector and another one in the inner reflector which was adjacent to the core were investigated, and appropriate target subassemblies were designed by using the MCNP and FISPACT-II codes. In the inner reflector case, the YH_2 moderator material was adopted for the neutron spectrum adjustment within the target subassembly. The gadolinia thermal neutron shielding is proposed to suppress the power peak of the adjacent fuel assembly. The result confirmed that a sufficient amount of ^{135}Cs can be produced at 1200 Effective Full Power Day (EFPD) in Joyo reactor (Mark IV core, 100 MWth).

1. Introduction

Radioactive nuclides such as minor actinides (MAs) and fission products (FPs) are produced in nuclear reactors. MAs are mainly produced by the radioactive capture reaction. FPs are produced by fission, and nuclides such as ^{79}Se, ^{93}Zr, ^{99}Tc, ^{107}Pd, ^{129}I, ^{135}Cs have long half-lives (more than 200,000 years) and are called long-lived fission products (LLFPs). FPs and MAs are categorized into high-level radioactive waste (HLW) and are subject to geological disposal in Japan, therefore, it would be beneficial to transmute LLFPs into short-lived radionuclides or stable elements to reduce the risk of radiation exposure (Partitioning and transmutation: P & T) (IAEA, 1982). The latest safety case report of Japan for the deep geological repository has shown that ^{129}I and ^{79}Se are the primary causes of potential radiation exposure in the far future, depending on the assumed scenario (NUMO, 2018a; NUMO, 2018b).

In the past, many simulation studies on the transmutation of LLFPs using nuclear reactors have been conducted (Arie et al., 2009; Ikegami et al., 2001; Naganuma et al., 2006; Sekimoto et al., 1998; Takaki et al., 2002, 2003, 2004; Yang et al., 2004). Recently, it has been shown that the transmutation of LLFPs is possible without isotope separation using a Monju (714MWt) class fast reactor (Chiba et al., 2017; Wakabayashi et al., 2019a; Wakabayashi et al., 2019b; Wakabayashi et al., 2020). A sodium-cooled fast reactor was selected in the studies because of its high excess neutrons and high neutron flux available for the transmutation. In this series of studies, the support ratio (SR: Destruction/Production) is used as a performance index to represent the transmutation capability of the nuclear reactor. A nuclide with an SR value of more than 1.0 can be reduced in the system, and on the contrary, if it is less than 1.0 it cannot be reduced by transmutation. The studies showed that the SR values for all LLFP nuclides are greater than 1.0, however, if the nuclear data uncertainties of 1σ are taken into account, there are possibilities that SR values for ^{79}Se, ^{93}Zr, and ^{135}Cs may be lower than 1.0 (Yamano et al., 2021). In other words, if the uncertainty of the SR (which originated from the nuclear data uncertainty of the capture cross-section) is too large then even when the best estimate of SR is just above 1.0, there is a possibility that the actual SR is less than 1.0 and the reactor system does not reduce the LLFP (but increase the LLFP). Therefore, the accuracy of the nuclear data of these LLFP

* Corresponding author.
E-mail address: liemph@nais.ne.jp (P.H. Liem).
[1] Present address: Tokyo Institute of Technology, 2-12-1 N1-12 Ookayama, Meguro-ku, Tokyo 152-850, Japan

https://doi.org/10.1016/j.anucene.2021.108830
0306-4549/

nuclides should be enhanced by measurements. To provide an adequate amount of samples for the measurement, one needs to investigate the LLFP target, irradiation assembly as well as irradiation fields in the useable fast reactor (in this case Joyo reactor).

To obtain reliable nuclear data for LLFP transmutation, one has to measure the neutron capture cross-section using the time-of-flight method, etc., and for the measurements, several hundred mg to 1 g of LLFP target material is required (Shcherbakov et al., 2005). In the case of LLFPs, however, it is difficult to procure such an amount of LLFPs. To cope with the problem, an irradiation test of natural cesium containing LLFP (^{135}Cs) in the burnup chain was devised. This study was carried out by simulation analysis assuming irradiation in the Japanese sodium-cooled fast experimental reactor "Joyo" (Maeda et al., 2005). In Joyo, an irradiation subassembly was loaded in the outer reflector region of the two-layer reflector to form an appropriate irradiation field (Aoyama et al., 2005).

In this paper, we report the results of the design study on the cesium target subassembly for two irradiation fields in the Joyo reactor. The first irradiation field is in the outer reflector region same as in the previous study (Aoyama et al., 2005). Loading the target subassembly into this location is recommended by the Joyo reactor group since it would not affect the reactor characteristics (as will be shown later), however, the neutron flux level is not high enough, especially for our cesium case. To provide a high neutron flux environment, we considered another irradiation field adjacent to the core, i.e. loading the test assembly in the inner reflector region in contact with the core most outer fuel subassembly. As will be shown later, we also incorporate moderator materials such as YH_2 and YD_2 in the target subassembly for spectrum adjustment. The use of YH_2 that has a strong moderating capability will induce higher power peaks in the adjacent fuel assembly. To resolve the problem, we propose the use of gadolinia thermal neutron shielding in the target subassembly design. The main goal or purpose of our design study is to obtain an irradiation test assembly (hereafter, test-assembly) loaded into an appropriate irradiation field that can provide a sufficient amount of ^{135}Cs. We expect this will contribute to the cross-section measurements for improving the nuclear data accuracy.

The structure of the paper is as follows. In Chapter 2 the Joyo reactor is briefly described. Chapter 3 describes the irradiation target, test assemblies, and loading positions proposed in the present design. In Chapter 4, the design and analysis method used are first explained, and then the analysis results are discussed. The conclusions of the present work are given in Chapter 5.

2. Experimental fast reactor Joyo

Joyo is the first FBR in Japan. It was constructed as an experimental reactor and achieved the initial criticality in 1977. The main

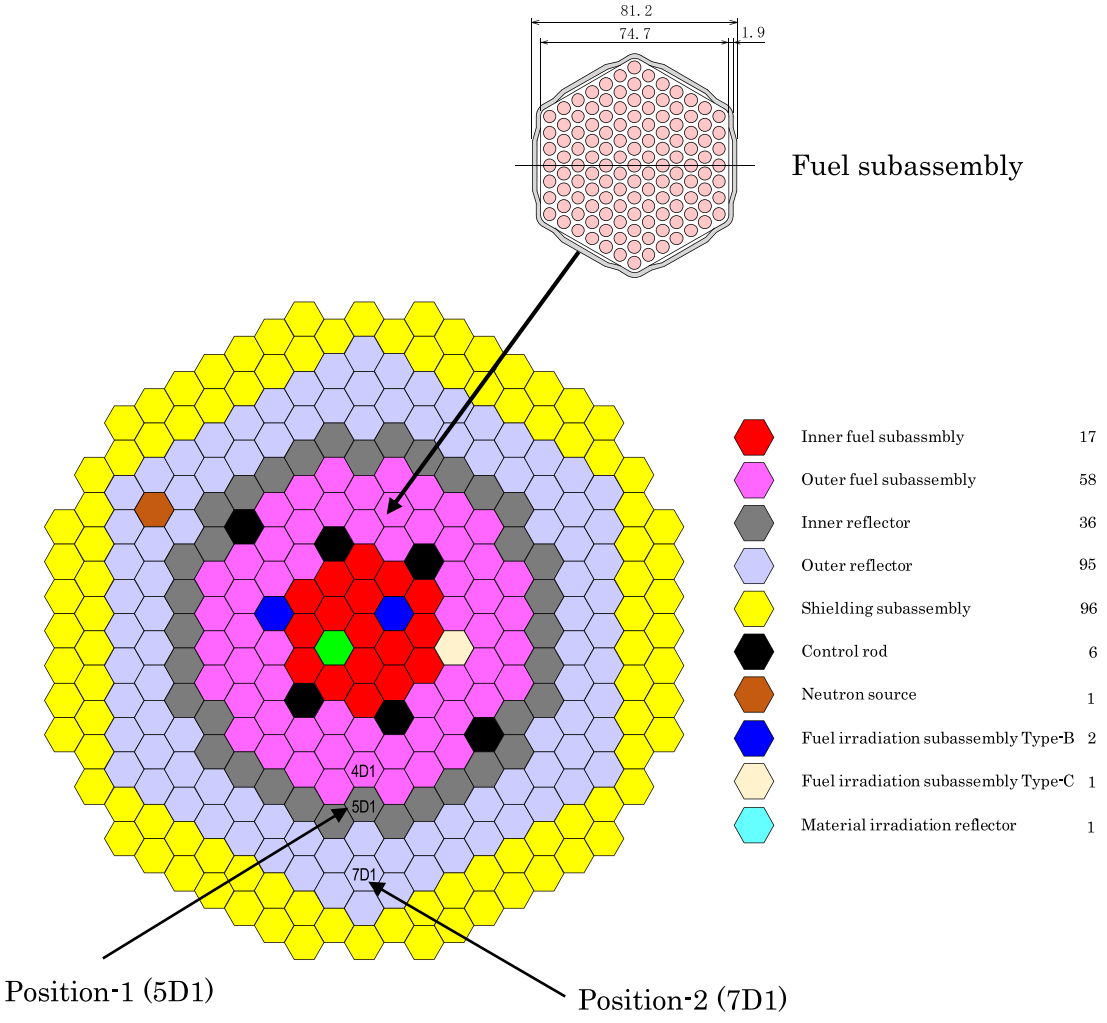

Fig. 1. Core configuration of Mark-IV and the loading positions for the test assemblies. The symbols of 5D1 etc. represent locations in the reactor core of Joyo.

Table 1
Main parameters of the Joyo Mark-IV core.

Parameters (Unit)	Values
Reactor thermal power (MWt)	100
Maximum number of fuel subassemblies*	79
Days per operation cycle (day)	60
Operation cycles per year	5
Active core height (cm)	50
Initial fuel density (%TD)	94
Maximum Pu Content: Pu/(Pu+^{241}Am + U) (wt%)	32
Fissile Pu content: (^{239}Pu+^{241}Pu)/(Pu+^{241}Am + U) (Inner/Outer) (wt%)	~16/~21
O/M ratio	1.97
Primary coolant temperatures (Inlet/Outlet)(°C)	350/456
Reflector /Shielding	SUS/B_4C
Control rod requirements (%Δk/k)	Maximum excess reactivity 2.0 (burnup1.4 + operating margin 0.6) Temperature and power compensation 1.49 (100 degrees C ~ rated power)
Irradiation period (EFPD)	1200
The chemical form of the target	Cs_2CO_3 (4.24 g/cm^3)
Moderators	YH_2, YD_2
Moderator volume ratio in the target pellet (%)	95
Diameter of the target rod (Outer/Inner) (mm)	8.5/7.5
Cladding thickness (mm) and material of the target rod	0.5/ SUS
Length of target pellets and number of target rods in the irradiation test-assemblies	
Test-assembly A	2.0 cm/ 1 rod
Test-assembly B	5.0 cm/ 37 rods

* Including the number of irradiation test fuel subassemblies

role of Joyo is the improvement of technology for a fast reactor, irradiation of fuel and material, and demonstration of innovative technology for putting a fast reactor into practical use (Maeda et al., 2014). In the future, reducing the volume and toxicity of radioactive waste (reducing environmental burden), studies on the safety of fast reactors, and basic technology as a neutron irradiation reactor, etc. are planned as operational targets of Joyo (Aoyama et al., 2005; Itagaki et al., 2017). Hence, the present study on irradiation experiments related to LLFPs is in line with the operational targets of Joyo. The transmutation experiments of MA/LLFP were also studied assuming irradiation in the prototype fast reactor Monju (Kitano et al., 2003), however, it was decided that Monju would be decommissioned (Nagaoki, 2020).

Joyo is planned to restart with enhanced safety levels reflecting the lessons learned from the Fukushima Daiichi Nuclear Power Plant accident. Its core is redesigned and called Mark-IV (100 MWt) (Itagaki et al., 2017). The core consists of two fuel regions (inner and outer regions), the reflector region and the shielding region. The fuel region has an equivalent diameter of approximately 78 cm and a height of 50 cm. The reflector region surrounding the fuels consists of three layers of stainless-steel subassemblies (one inner reflector and two outer reflectors). Shielding subassemblies with B_4C are loaded in the two outermost layers. The Mark-IV core configuration is shown in Fig. 1 and the main parameters of the core specifications are listed in Table 1. The irradiation fields at the positions where the irradiation test subassembly (hereafter, test-assembly) is loaded, i.e. Position-1 and Position-2 shown in Fig. 1 were examined.

3. Irradiation target, test assemblies, and loading positions

3.1. Irradiation target

Since LLFPs are produced from fissions in a nuclear reactor and extracted through chemical separation and refinement, it is difficult to get a sufficient amount of LLFP needed for an irradiation experiment such as a nuclear cross-section measurement. Accordingly, we decided to irradiate a natural element that produces an LLFP nuclide as its isotope. Stable nuclides included in such a natural ele-

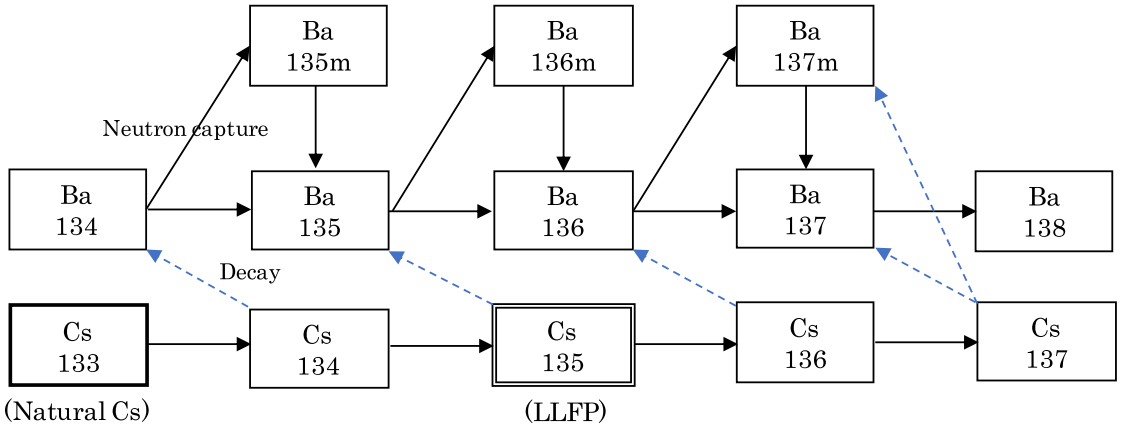

Fig. 2. Neutron capture and decay chains of Cs and Ba isotopes.

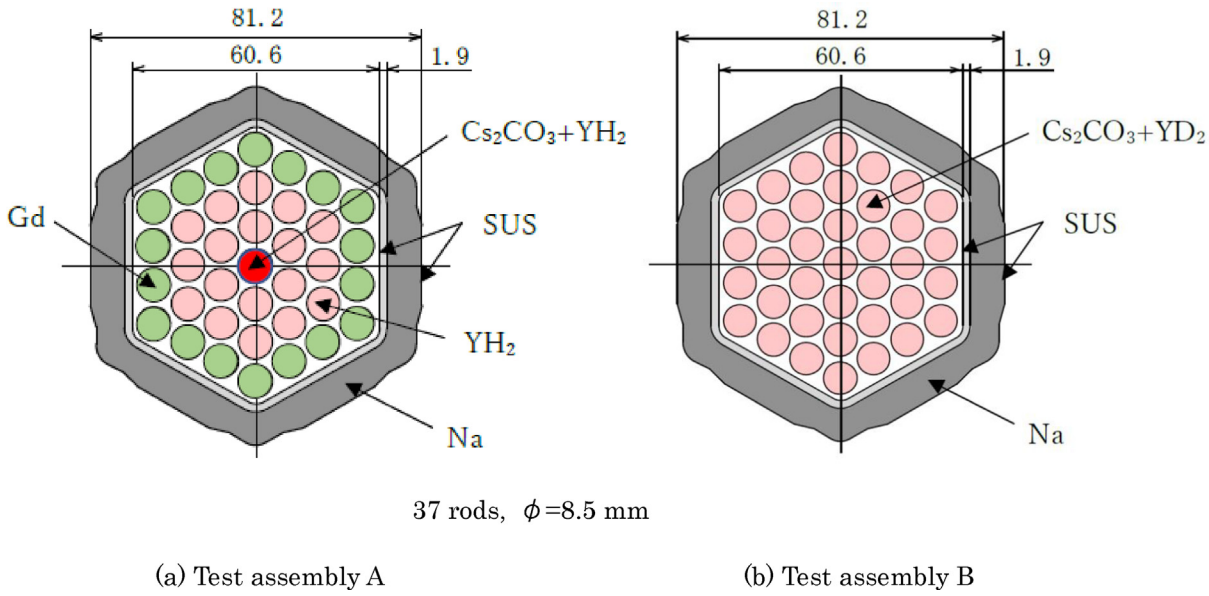

Fig. 3. Irradiation test assemblies.

ment need to have large capture cross-sections to produce a sufficient amount of LLFP. Also, to produce the LLFP nuclide efficiently, the maximum number of times of consecutive neutron capture reactions to reach the LFPP nuclide should be limited to two.

As the element and the LLFP nuclide which can meet such requirements, we selected natural cesium (which consists of only ^{133}Cs) and ^{135}Cs (See Fig. 2). Based on the JENDL-4.0 nuclear data (Shibata et al., 2011), the thermal capture cross-section of ^{133}Cs is 28.90 (b) and that of ^{134}Cs is 140.6 (b), while the resonance integral of ^{133}Cs is 446.2 (b) and that of ^{134}Cs is 72.50 (b). The thermal capture cross-section and resonance integral of the LLFP ^{135}Cs is 8.302 (b) and 53.52 (b), respectively.

Cesium carbonate (Cs_2CO_3) was selected as the chemical form of cesium because of its high dissociation temperature. Yttrium hydride (YH_2) was used as a moderator to soften the neutron spectrum and increase the transmutation rate, and the irradiation target was assumed to be a homogeneous mixture of Cs_2CO_3 and YH_2. The volume ratios of Cs_2CO_3 and YH_2 were determined to be 5% and 95%, respectively, by a pin cell calculation with a buffer region simulating Joyo's in-core neutron spectrum to maximize the amount of ^{135}Cs produced.

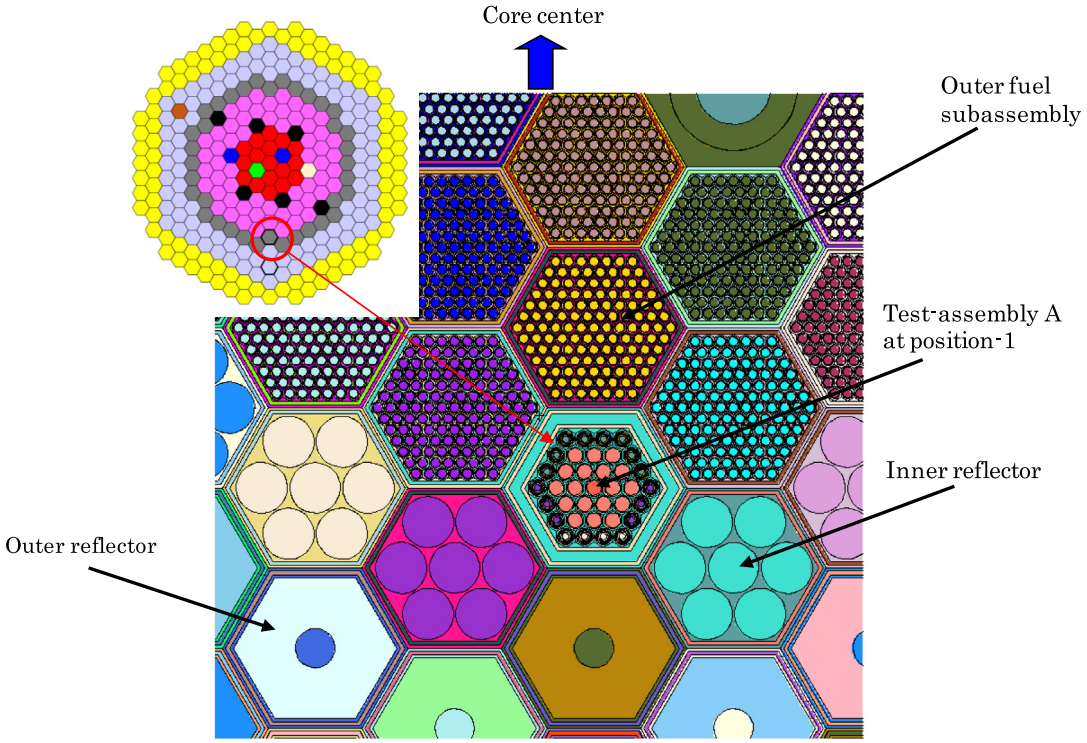

Fig. 4. Core configuration around Position-1.

3.2. Irradiation test assemblies and loading positions

The two test assemblies designed for neutron irradiation are shown in Fig. 3. The test-assembly A is loaded in Position-1 (5D1 in Fig. 1) and the test-assembly B is loaded in Position-2 (7D1 in Fig. 1). Since Position-1 is next to the fuel subassembly the high neutron flux can be utilized for transmutation. The three surfaces of the test assembly face the fuel subassemblies and the other three surfaces face the reflector subassemblies made of stainless steel. Yttrium hydride YH_2 is employed as a moderator to achieve a high transmutation rate even in a narrow region like the test assembly with a width of about 8 cm. However, some of the moderated neutrons leak out of the test assembly and significantly increase the power of the surrounding fuel rods. To avoid such power peaks, gadolinia rods for shielding thermal neutrons are placed in the outermost layer of the test-assembly A. Fig. 4 shows the detailed core configuration around Position-1.

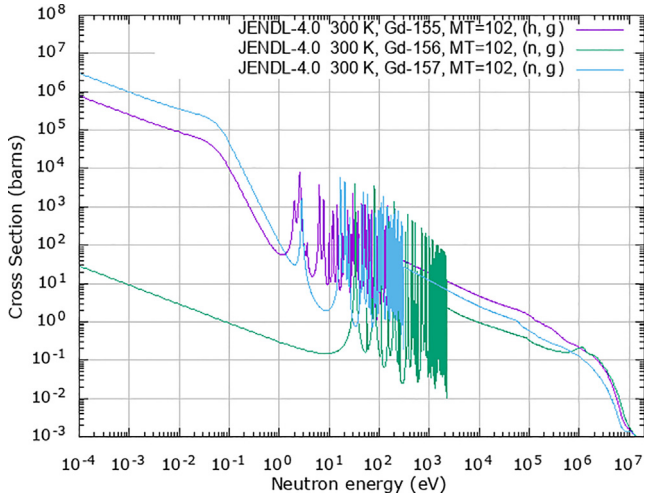

Fig. 5. Neutron capture cross-sections for ^{155}Gd, ^{156}Gd, and ^{157}Gd (JAEA, 2021).

As can be seen from Fig. 5, the neutron capture cross-sections of ^{155}Gd and ^{157} Gd are very large in the thermal energy region, but small in the fast energy region. This means that fast neutrons from the fuel region enter the inside of the test assembly without being absorbed by the gadolinia (Gd_2O_3) rods (hereafter, Gd rods) and are used for transmutation after being thermalized but thermal neutrons leaking from the test assembly without contributing to the transmutation are absorbed by them. As a result, the power peak due to the thermal neutrons can be suppressed.

As shown in Fig. 1, Position-2 is relatively far from the fuel subassembly compared to Position-1, so the moderator has a small effect on fuel pin power, and various types of moderators can be used (Aoyama et al., 2005). Fig. 6 shows the core configuration around the test-assembly B loaded at Position-2. The total neutron flux at this position is 1/3 of that at Position-1. Therefore, at Position-2, the utilization of intermediate energy neutrons is suitable for transmuting without decreasing neutron flux. For this reason, aluminum is selected as the moderator. Fig. 7 shows the cross-sections of ^{27}Al and ^{133}Cs. From this figure, it can be seen that aluminum has a small scattering cross-section that is almost constant but has a relatively large resonance scattering cross-section

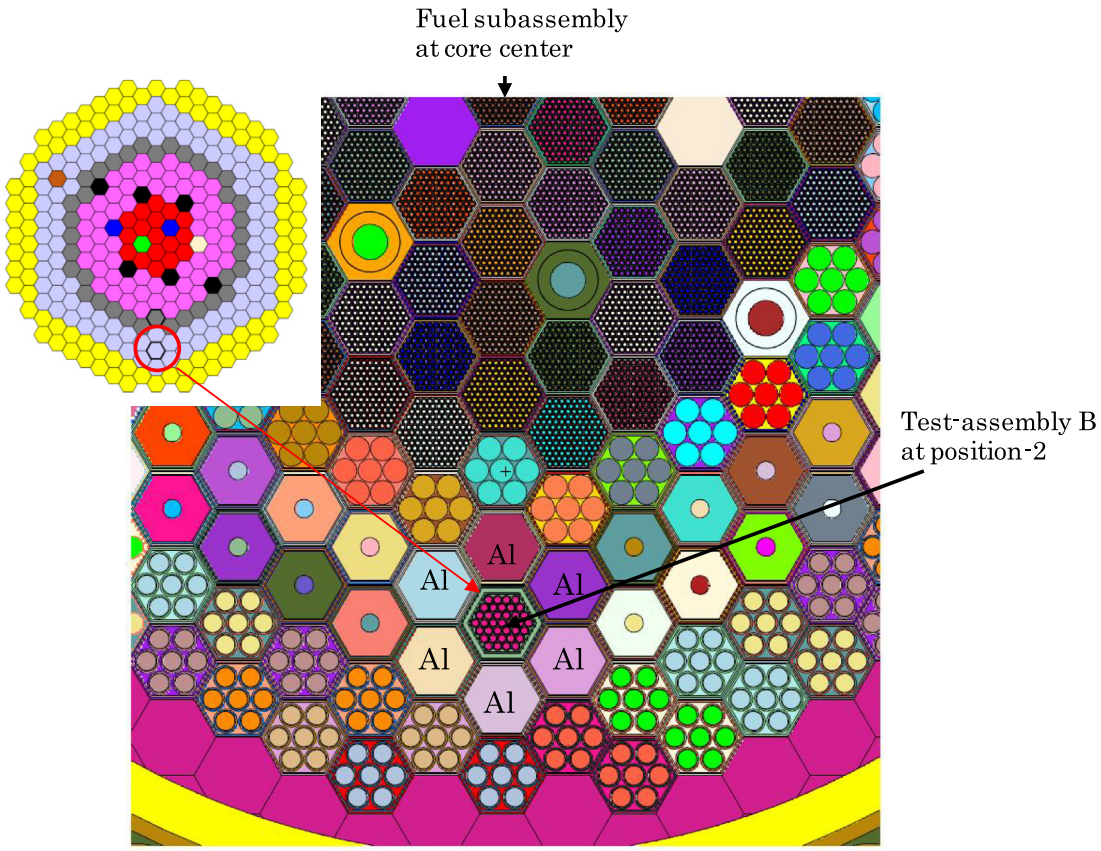

Fig. 6. Core configuration around Position-2.

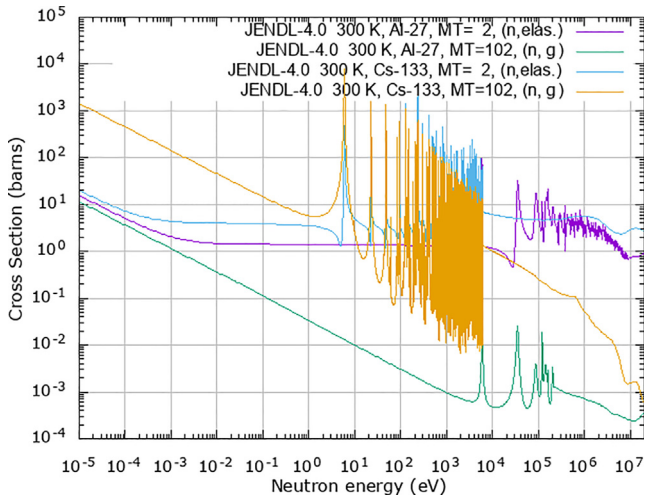

Fig. 7. Neutron capture and scattering cross-sections for ^{27}Al and ^{133}Cs (JAEA, 2021).

in the energy range exceeding 10^4 eV. From this, it is expected that aluminum slows fast neutrons down into the resonance energy region and forms an intermediate energy spectrum.

Six aluminum blocks (Al) are placed around the test-assembly B to form an intermediate energy neutron spectrum. Furthermore, yttrium deuteride (YD_2), which has a smaller neutron capture cross-section than YH_2, is used as the moderator for test-assembly B so that the neutron flux would not decrease.

4. Design and analysis results

4.1. Design and analysis method

The neutronics calculations were performed in a three-dimensional, fully heterogeneous core model using the Monte Carlo code MCNP6.2 (LANL, 2017) and the nuclear data library JENDL-4.0. The number of effective neutron histories is 50 million. Under this calculation condition, the worst uncertainty of the total flux tally at the Cs targets is less than 0.83 % and 0.35 % for the irradiation Position-1 and 2, respectively, while the uncertainty of the

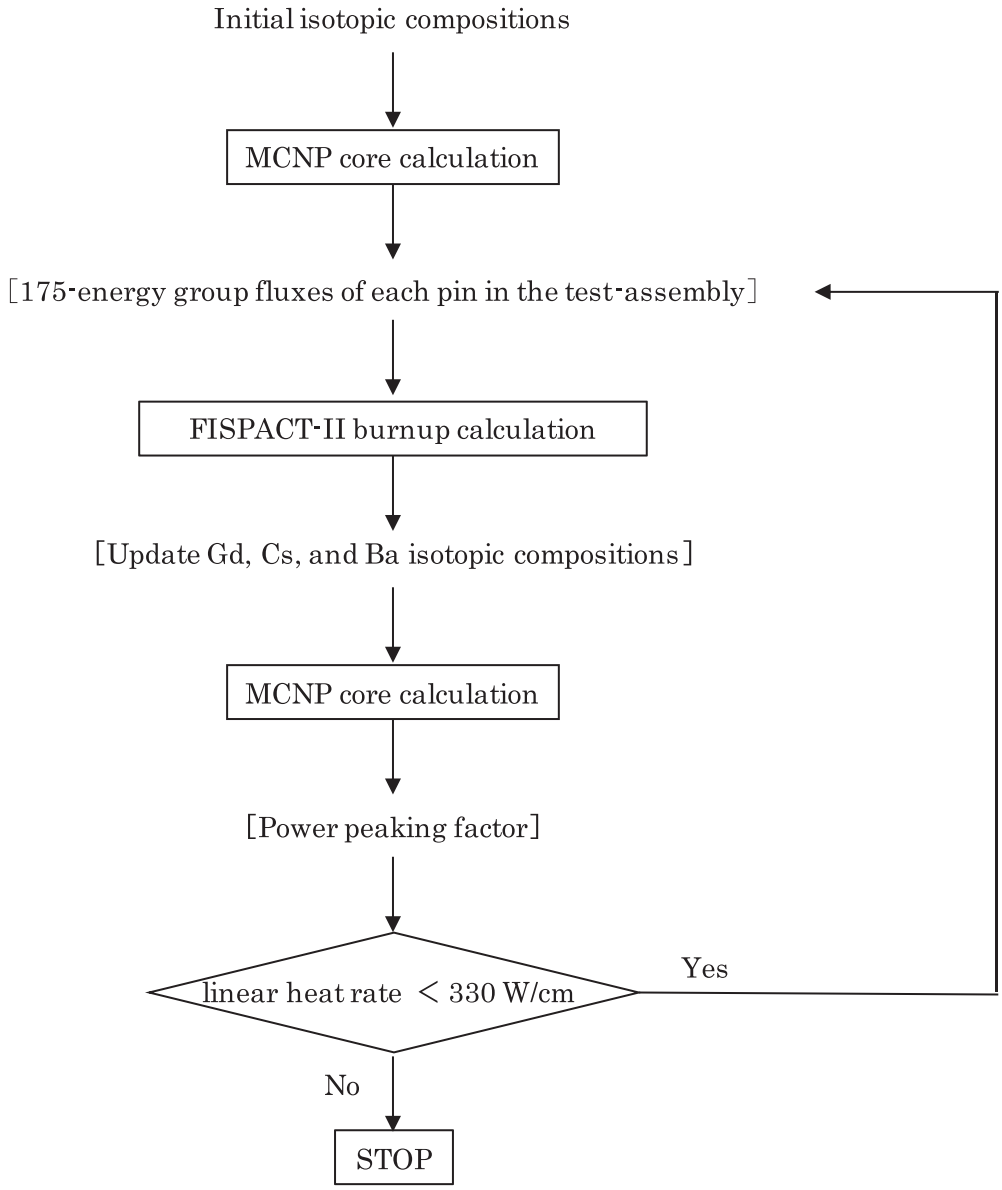

Fig. 8. Schematic flow diagram of burnup calculation.

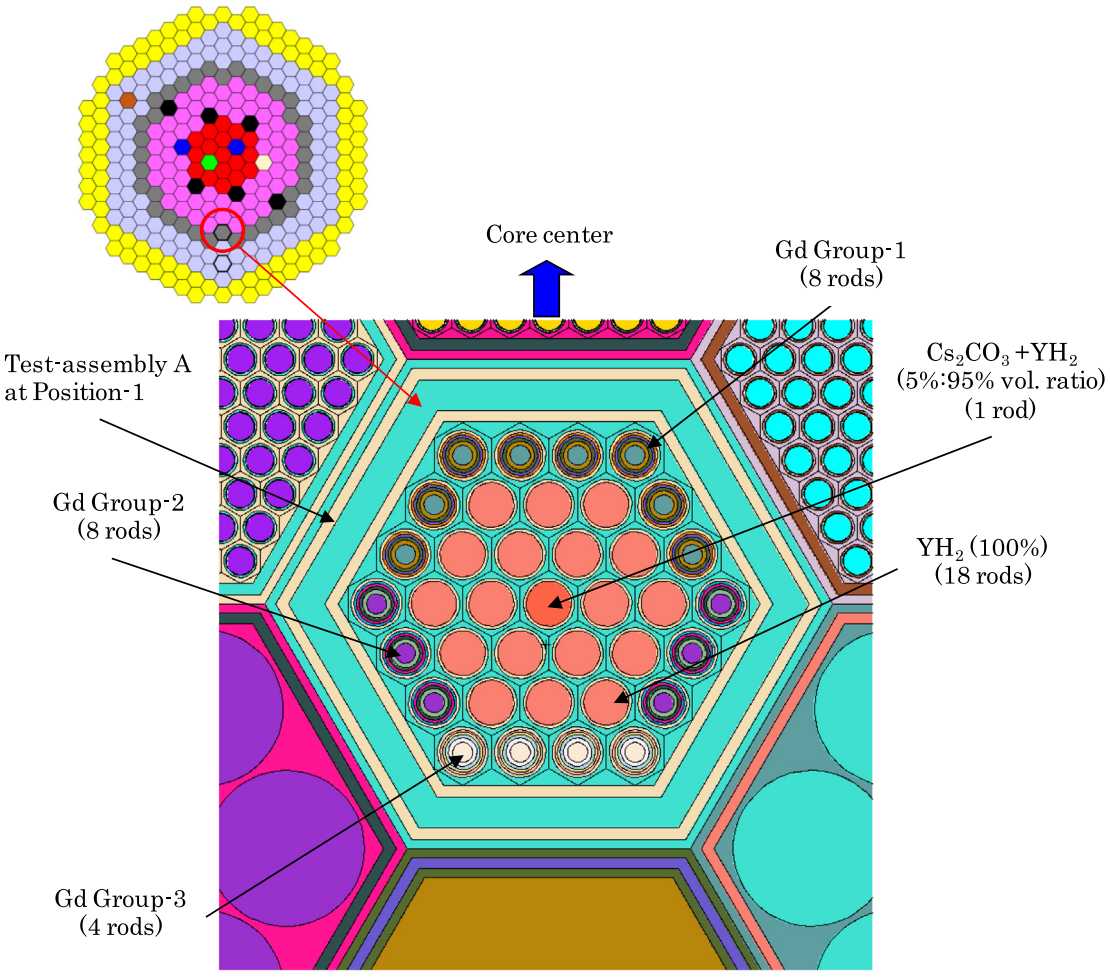

Fig. 9. Fine spatial divisions and groupings of Gd rods for tallying in the test-assembly A.

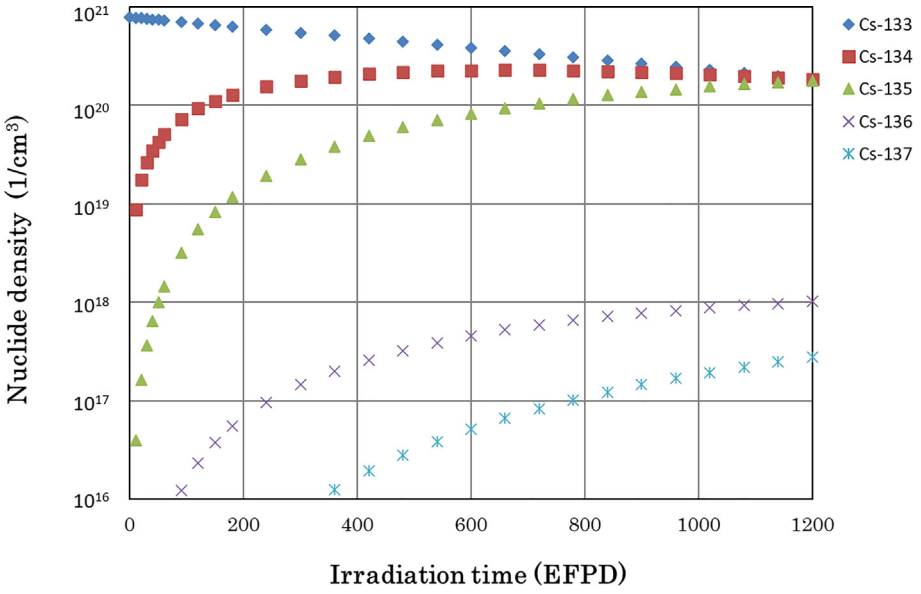

Fig. 10. Change in Cs isotopes with the irradiation time at Position-1.

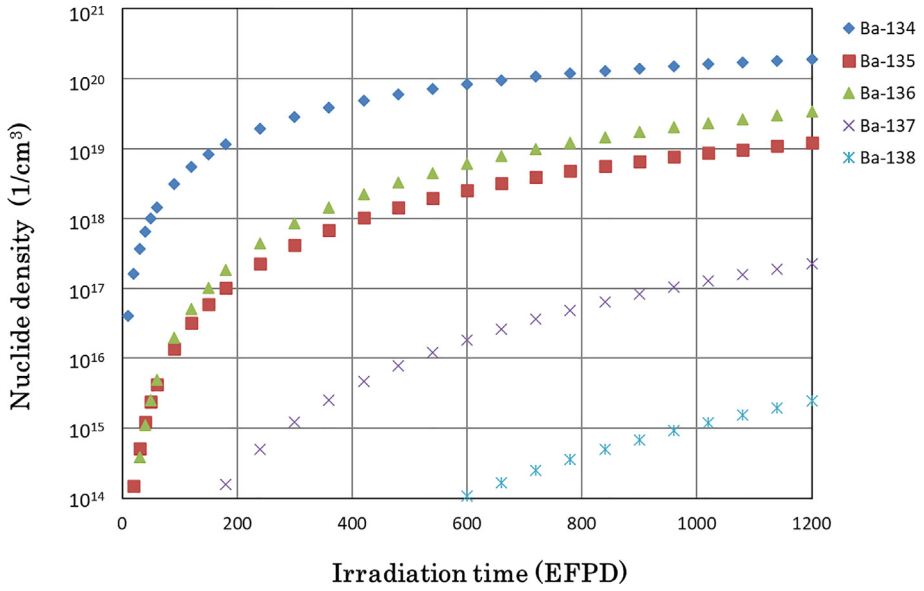

Fig. 11. Change in Ba isotopes with the irradiation time at Position-1.

effective multiplication factor (k_{eff}) is about 8 pcm. The fuel compositions are those at the beginning of the equilibrium cycle of the Joyo Mark-IV core. It should be noted that for a typical fast reactor like Joyo, the core compositions at the beginning and the end of the equilibrium cycle will not differ significantly, therefore, the core composition at beginning of the equilibrium cycle is taken as the representative composition for the present study.

The compositions of Cs, Ba, and Gd were calculated with FISPACT-II 3.20 (Fleming et al., 2018) using the VITAMIN-J 175-energy-group spectra (Sublet et al., 2016) and the flux levels, which were obtained from the MCNP core calculations. As a self-shielding method, the universal curve model in FISPACT-II was used in the calculation. Since the isotopic compositions change with burnup, the fuel rod power peaks of the subassemblies adjacent to test-assembly A were calculated by MCNP using the isotopic compositions obtained after each burnup calculation. Thus, the MCNP core calculation and the subsequent FISPACT-II burnup calculation are repeated to proceed with burnup. Fig. 8 shows a schematic flow diagram of the burnup calculation using MCNP and FISPACT-II. The irradiation period is up to 1200 effective full power days (EFPDs). This irradiation time corresponds to 4 years under the conditions of 60 days per cycle at rated power and 5 cycles per year. The burnup step is determined by first observing the time behaviors of the LLFP and gadolinium isotopes under a constant neutron flux spectrum and level. If the nuclides change rapidly during the time interval initially set, it is changed to the shorter one. In real calculations, these variable time steps are adopted to produce accurate burnup calculation results.

4.2. Criticality analysis results

The test assembly is loaded into the position of either Position-1 or Position-2. The core without any test assemblies is the reference core which consists of 75 fuel subassemblies. The control rods are at the position of 505 mm from the bottom of the core; the control rod position fully withdrawn is 650 mm. The control rods were fixed to this position in all the core calculations. The effective multiplication factors (k_{eff}) are shown below,

$k_{eff} = 1.00100 \pm 0.00008$ for no test-assembly (Reference),

$k_{eff} = 0.99847 \pm 0.00008$ for test-assembly A in Position-1,

$k_{eff} = 1.00017 \pm 0.00008$ for test-assembly B in Position-2.

The reactivity of the core in which the test-assembly A is loaded is low by 0.25 % against the reference core. This reactivity loss is within the reactivity margin of 0.6% set for control rod maneuver as shown in Table 1 and thus can be compensated by the control rods.

4.3. Burnup analysis results

4.3.1. Results at Position-1

The material configuration in the test-assembly A loaded at Position-1 and fine spatial divisions and groupings of gadolinia rods are shown in Fig. 9. This figure reflects the MCNP calculation model. The center pin contains the homogeneous mixture of Cs_2CO_3 and the moderating material YH_2 and is surrounded by eighteen moderator pins, which have only YH_2. In the outermost layer, eighteen gadolinia rods are loaded.

Special attention was paid to the gadolinium burnup calculation because the gadolinium isotopic compositions vary very rapidly with burnup and their distributions in the pellet strongly depend on the spatial self-shielding of neutron absorption. Accordingly, each gadolinia pin was divided into five equal-volume areas as tally regions in a burnup calculation to obtain a reliable result. Fine time steps were employed for the neutron spectrum and flux reevaluation in each region in each pin at the early stage of the burnup calculation. Furthermore, since the burnup of gadolinium isotopes strongly depends on the thermal flux, the Gd rods were grouped into three as shown in Fig. 9. The neutron population was tallied in each group in burnup calculations.

The change in Cs isotopes with the irradiation time is shown in Fig. 10. This figure shows that ^{135}Cs nuclide is produced to the amount of about 10% of the initial ^{133}Cs (natural cesium) at 600 EFPDs, and at 1200 EFPDs it becomes comparable to the amount of the residual ^{133}Cs.

The change in Ba isotopes with the irradiation time is shown in Fig. 11. The production of ^{134}Ba at 1200 EFPDs is almost equal to the residual amount of ^{133}Cs. The production of ^{135}Ba and ^{136}Ba is lower than that of ^{134}Ba approximately by a factor of 10. The measured amounts of ^{134}Ba、^{135}Ba、and ^{136}Ba can be used as sup-

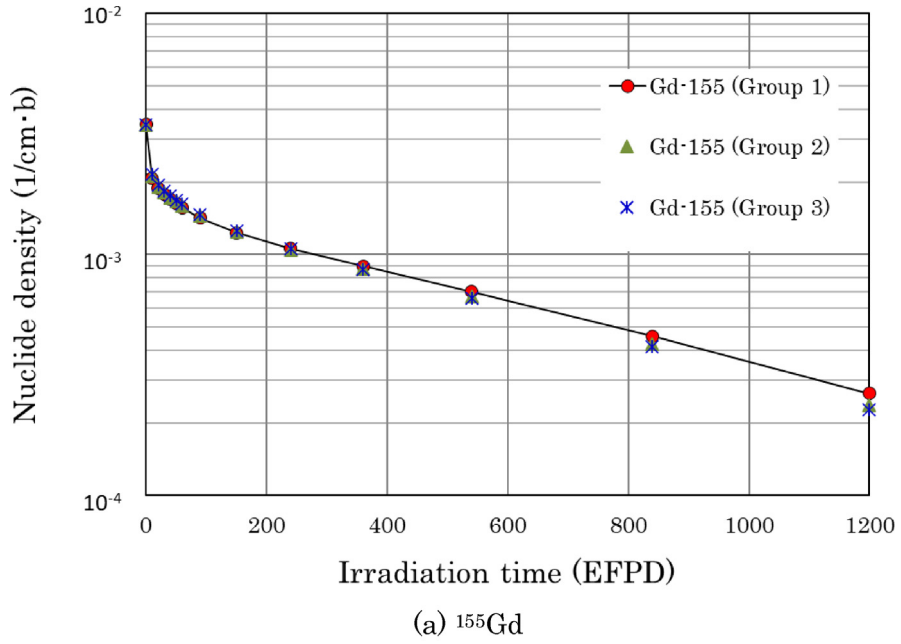

(a) ^{155}Gd

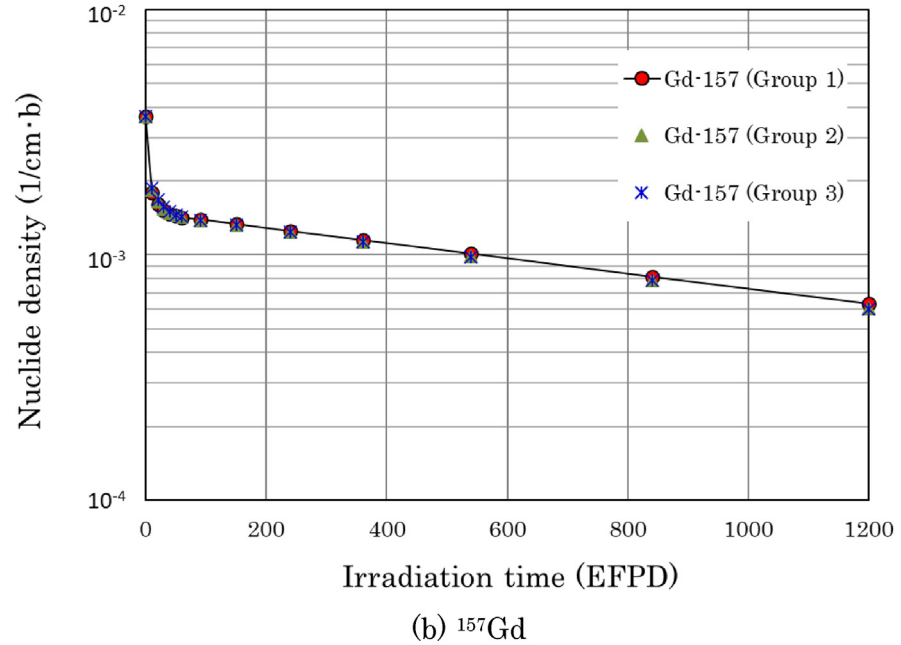

(b) ^{157}Gd

Fig. 12. Gadolinium isotope concentrations in the test-assembly A as a function of the irradiation time. Group 1, 2, and 3 indicate the grouping of Gd rods shown in Fig. 9.

plementary data in the evaluation of the (n, γ) reaction rates of ^{133}Cs and ^{134}Cs.

Fig. 12 shows the change in ^{155}Gd and ^{157}Gd isotopes as a function of the irradiation time. The ^{155}Gd concentration decreases to about half of its initial value at the burnup of 40 EFPDs and becomes less than 1/10 at 1200 EFPDs. On the other hand, the ^{157}Gd concentration becomes half after the burnup of about 14 EFPDs, which is earlier than ^{155}Gd, but its residual amount at 1200 EFPDs is larger than that of ^{155}Gd. Thus, it is seen that the change of ^{157}Gd with burnup is not large than that of ^{155}Gd. This is because the depletion of ^{157}Gd is compensated by the production from ^{156}Gd (n, γ) reactions in the burnup chain of Gd isotopes as shown below.

$$64152Gd \underset{(n,\gamma)}{\rightarrow} 64153Gd \underset{(n,\gamma)}{\rightarrow} 64154Gd \underset{(n,\gamma)}{\rightarrow} 64155Gd \underset{(n,\gamma)}{\rightarrow} 64156Gd \times \underset{(n,\gamma)}{\rightarrow} 64157Gd \underset{(n,\gamma)}{\rightarrow} 64158Gd \underset{(n,\gamma)}{\rightarrow}$$

From these, it is found that the role of Gd to suppress the power peaking can be maintained for a considerably long period.

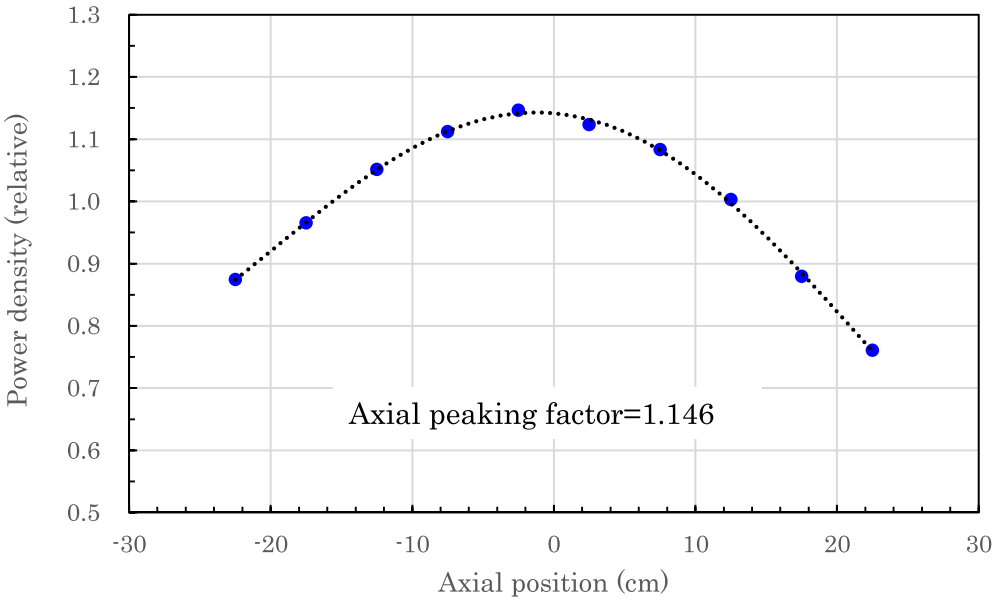

Fig. 13. The axial power distribution of the hot assembly. The mean power of this assembly is normalized to 1.0.

Table 2
Evaluation of peaking factors and maximum linear power densities.

Burnup(EFPD)	Peaking factor*					Linear powerDensity	Remarks
	F_A	F_{Rod}	F_R	F_z	F_Q	q'_{max}(W/cm)	
0	1.006	1.784**	1.795	1.146	2.057	432	Without Gd rods
0	0.890	1.086***	0.967	1.146	1.108	233	With Gd rods
540	0.918	1.126**	1.034	1.146	1.185	249	
1200	0.924	1.149**	1.062	1.146	1.217	256	

* The definitions of the peaking factors are shown in Sec. 4.3.
** The peak power occurs in fuel neighboring to the test-assembly A (Fig. 14).
*** The power peak appears on the opposite side of the fuel subassembly surface on which the test-assembly A is neighboring (Fig. 15).

The power peak occurs in the fuel subassembly (4D1 in Fig. 1) next to the test-assembly A and its value will increase with burnup because of ^{155}Gd and ^{157}Gd depletion. The linear power density, however, must not exceed its design limit of 330 W/cm in Joyo to avoid fuel melting. Therefore, the linear power densities were evaluated using the power peaking factors obtained by the simple synthesis method.

$$F_A = Assembly\ relative\ power\ in\ the\ core\ (hot\ subassembly)$$
$$F_{Rod} = Maximum\ rod\ power\ normalized\ in\ the\ subassembly$$
$$F_R = Radial\ peaking\ factor\ = F_A \cdot F_{Rod}$$
$$F_Z = Axial\ peaking\ factor$$
$$= \frac{Maximum\ linear\ power\ density\ of\ hot\ subassembly}{Mean\ linear\ power\ density\ of\ hot\ subassembly}$$
$$F_Q = Power\ peaking\ factor = F_R \cdot F_Z = (F_A \cdot F_{Rod}) \cdot F_Z$$

The power peaking factors F_A, F_{Rod}, and F_Z are obtained from the MCNP calculation results. The axial power peaking factor F_Z is defined as the ratio of peak to average assembly power density for the hot subassembly having the power peak, and its value is 1.146 from the axial power distribution shown in Fig. 13. This value of Fz was used for all the power peaking factor calculations.

Since the Mark-IV core accommodates 75 fuel subassemblies and each fuel subassembly has 127 fuel rods, the mean linear power density q' is, assuming the total thermal energy is generated in the inner and outer fuel subassemblies for conservative evaluation,

$$\langle q' \rangle = \frac{100(MW) \times 10^6}{127(rods/subassembly) \times 75(subassembly) \times 50(cm)}$$
$$= 210\ W/cm$$

Using the power peaking factor and the mean linear power density, the maximum linear power density is evaluated as

$$q'_{max} = \langle q' \rangle \cdot F_Q$$

The power peaking factors and the maximum linear power densities are summarized in Table 2. In the case without Gd, all the Gd rods were replaced with YH_2 moderator rods. The normalized pin power (distribution) is shown in Fig. 14 and the maximum one (F_{ROD}) is as high as 1.784. This large F_{ROD} causes a large linear power density of 432 W/cm, which exceeds the design limit of 330 W/cm. On the other hand, when Gd rods are used as shielding of thermal neutrons, the power of the same fuel rod reduces to

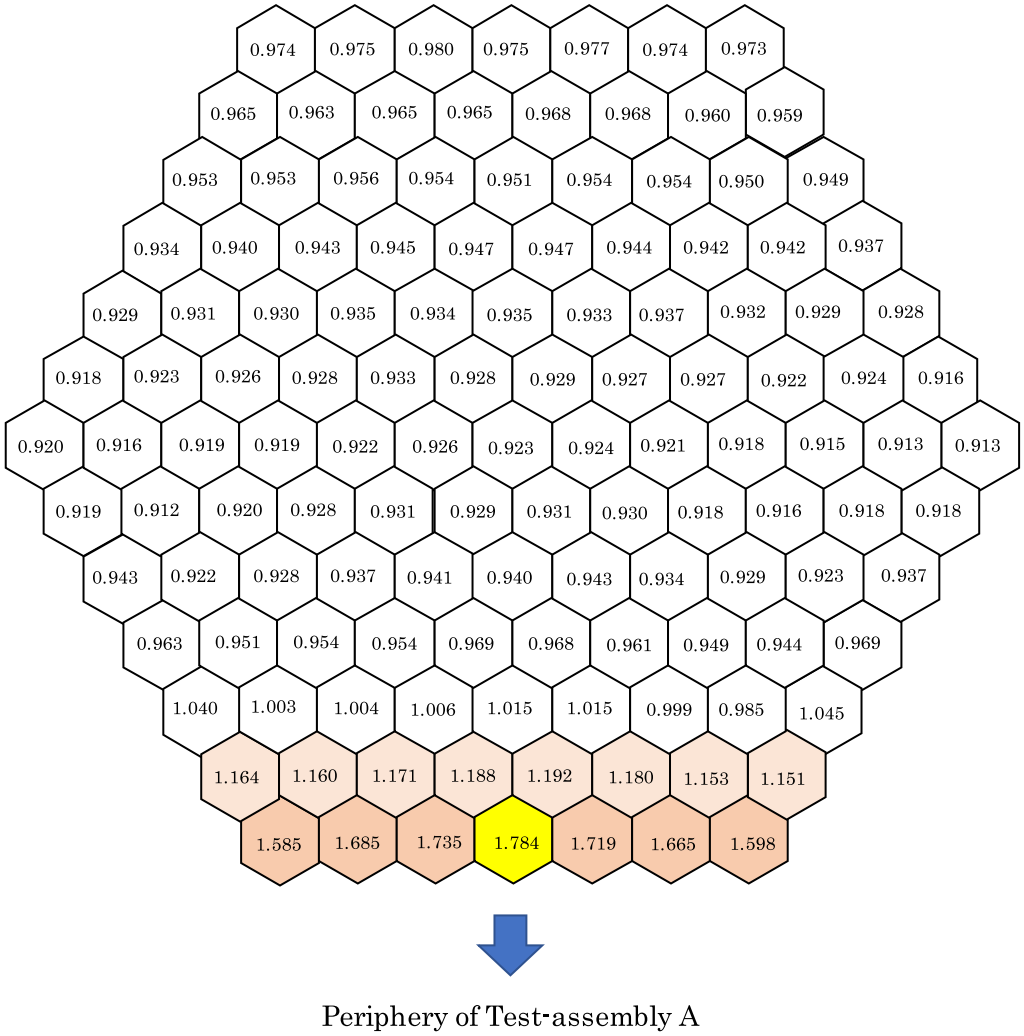

Fig. 14. Pin power distribution in the hot assembly when the test-assembly A has no Gd rods. (Gadolinium rods are replaced with YH_2 moderator rods.)

1.026 as shown in Fig. 15. In this case, the peak power of this fuel assembly appears on the opposite side and F_{ROD} is 1.086 from Fig. 15. From the burnup calculation results in Table 2, it is seen that the linear power density is 256 W/cm even at 1200 EFPDs (although the gadolinium rods have already been irradiated considerably) and meets the design requirement. This demonstrates that the utilization of Gd rods is effective in suppressing power peaks while achieving a high transmutation rate.

Neutron spectra of the target pellet (YH_2 + Cs_2CO_3) in energy and lethargy representations are shown in Fig. 16. The neutron spectrum in energy representation increases monotonically in logarithmic scale in the energy range from 1 MeV to about 0.6 eV. Further, since a small thermal peak appears in the energy range between 0.01 eV and 0.1 eV neutrons are found to be thermalized. On the other hand, the neutron spectrum in the lethargy representation simply decreases with decreasing neutron energy in the same energy region. Observing neutron spectra within the Gadolinia pellets shown in Fig. 17, the flux level of the neutron spectra is much lower than that shown in Fig. 16 for neutron energies below 1 eV and have no thermal peak. From this fact, one can conclude that gadolinia effectively works as thermal neutron shielding.

4.3.2. Results at Position-2

The placement of the test-assembly B and Al blocks at Position-2 is shown in Fig. 18. The test-assembly B has 37 target pins that contain the mixture of Cs_2CO_3 and YD_2, and it is surrounded by six aluminum blocks. The core power peak is not an issue because this position is far from fuel subassemblies and the yttrium deuteride (YD_2) having lower slowing down power than YH_2 is used as a moderating material. As expected, the power peaking factor was as low as 1.19.

The change in Cs isotopes with the irradiation time is shown in Fig. 19. The production of LLFP ^{135}Cs nuclide is about 1/1000 times the initial amount of ^{133}Cs (natural cesium) at 600 EFPDs and at 1200 EFPDs it reaches 1/100. The change in Ba isotopes with the irradiation time is shown in Fig. 20. Compared to Fig. 11 at Position-1 the production of the Ba isotopes is 1/10 to 1/100. The reason why the production is so small is due to the low neutron flux. That is, the total flux at Position-2 is 6.0×10^{14} $cm^{-2}s^{-1}$ and about 3 times lower compared to that of 1.8×10^{15} $cm^{-2}s^{-1}$ at Position-1. The neutron spectra are shown in Fig. 21.

The production of ^{135}Cs (initial loading and production) is summarized in (Table 3). The production rate of ^{135}Cs is 7.17 %/EFPY at

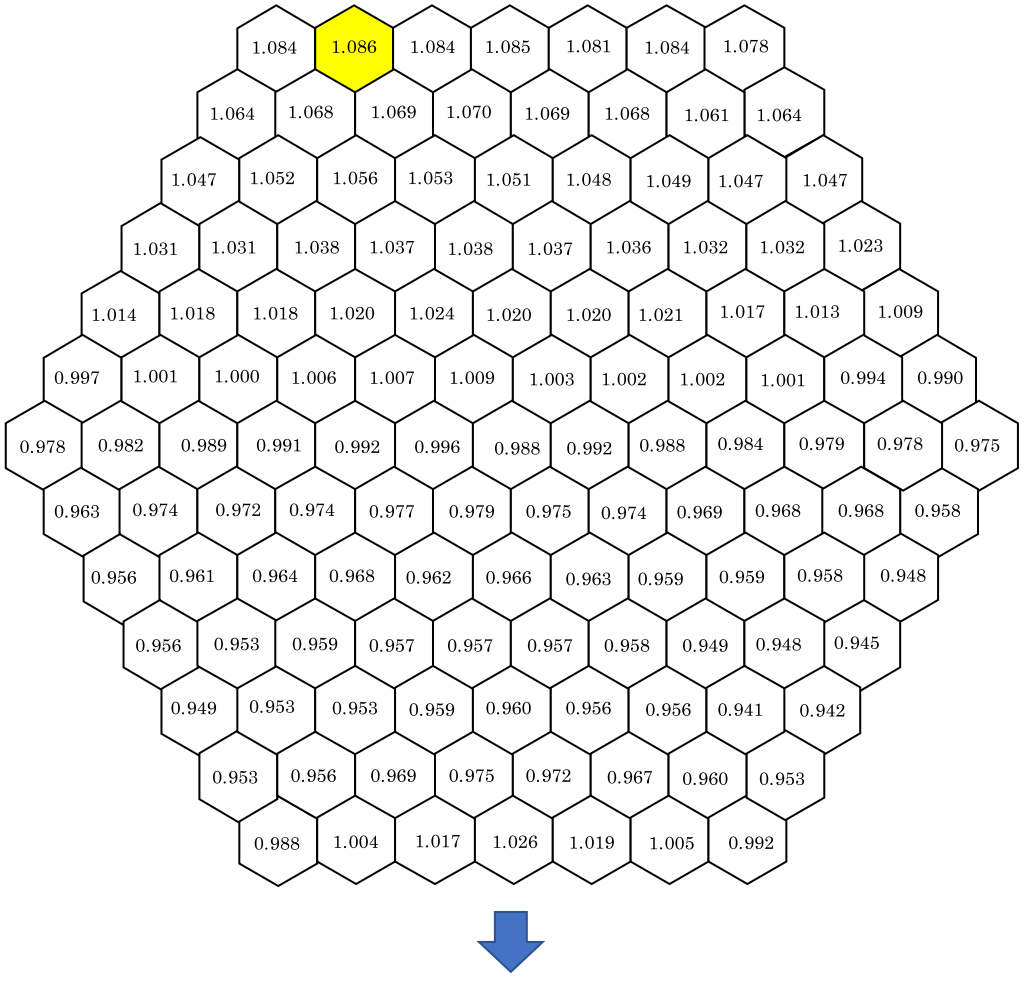

Fig. 15. Pin power distribution in the hot assembly when the test-assembly A has Gd rods.

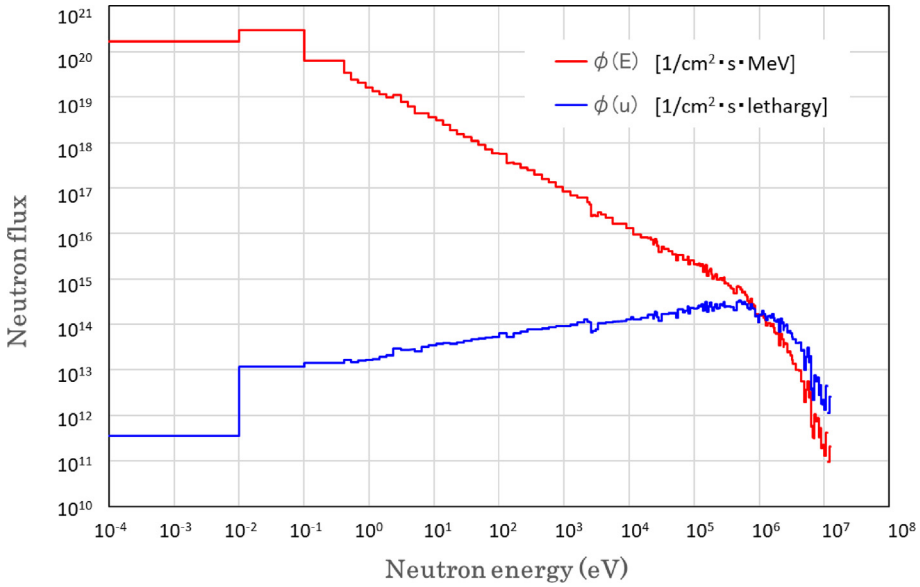

Fig. 16. Neutron spectra of the target pellet (Cs_2CO_3 + YH_2) of the test-assembly A.

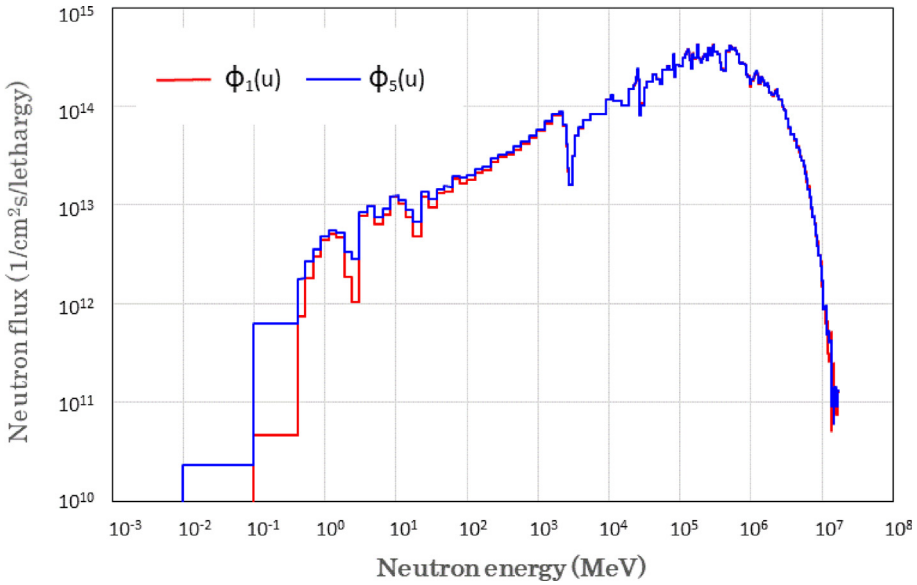

Fig. 17. Neutron spectra within the Gd pellets belonging to Group-1. Neutron spectra are denoted by φ_1 to φ_5 from the inside of the pellets toward the outside.

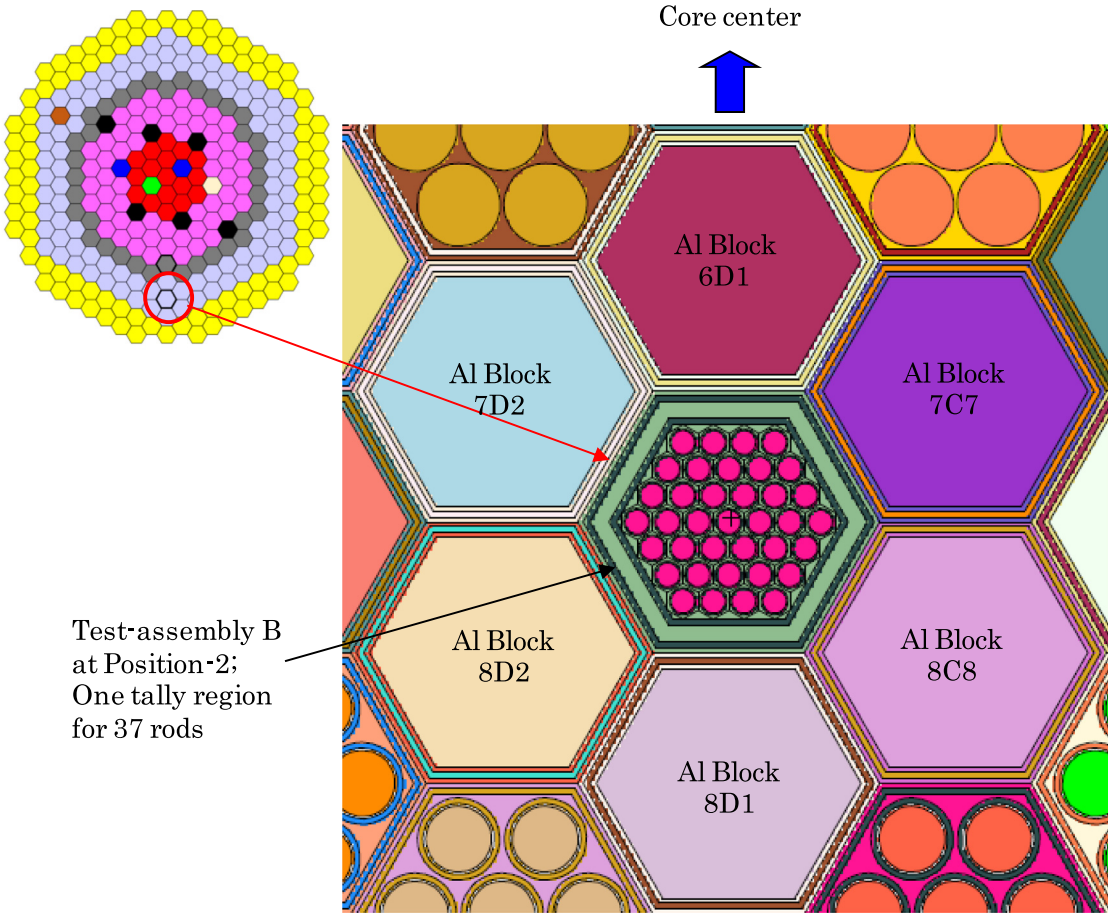

Fig. 18. Test-assembly B and the Al blocks at Position-2. The symbols of 6D1 etc. represent locations in the reactor core of Joyo.

Position-1 and 0.22 %/EFPY at Position-2. As mentioned before, the production rate at Position-2 is low because of the low flux level and may not be considered further in the future. On the other hand, the ^{135}Cs production capability at Position-1 can be potentially increased by (1) using all 19 rods of YH_2 + Cs_2CO_3, (2) increasing the target height from 2.0 cm to the needed length, to provide an adequate amount for cross-section measurements. Extending the irradiation time more than 1200 days may not increase

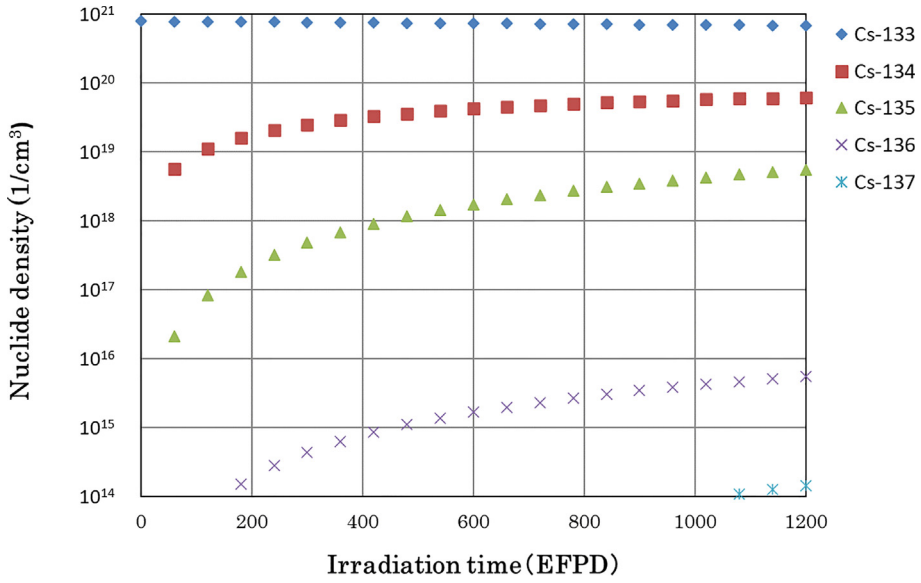

Fig. 19. Change in Cs isotopes with the irradiation time at Position-2.

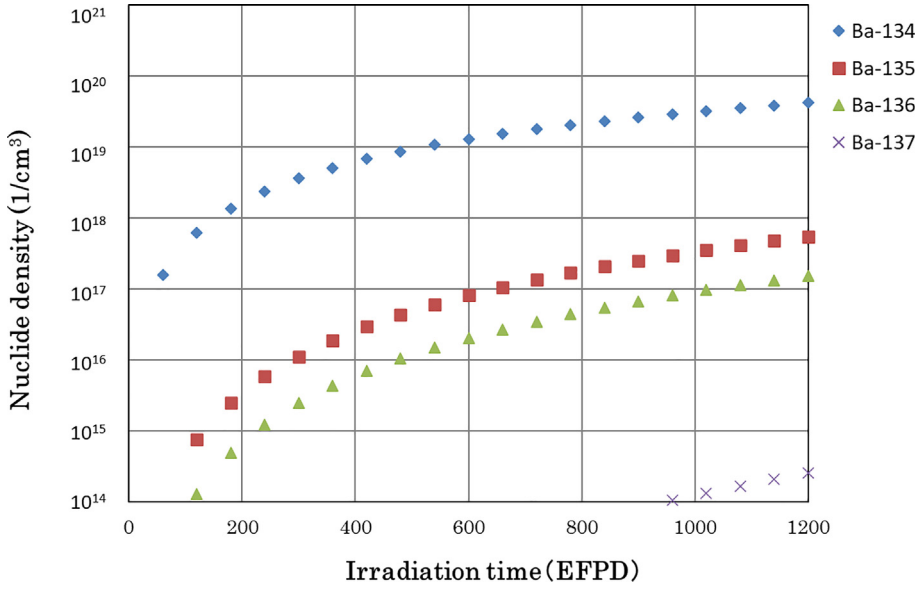

Fig. 20. Change in Ba isotopes with the irradiation time at Position-2.

significantly the production capability (cf. Fig. 10). Measurement of isotopes of Cs and Ba in PIE will allow validating the cross-sections of the $^{133}Cs(n,\gamma)^{134}Cs$ and $^{134}Cs(n,\gamma)^{135}Cs$ reactions through the burnup analysis.

5. Conclusions

Two irradiation fields in the inner (Position-1) and outer reflector (Position-2), and their corresponding target subassembly (Test-assembly A and B) designs to produce a sufficient amount of ^{135}Cs in the Joyo reactor (Mark-IV core, 100 MWth) were investigated. The investigation results show that a sufficient amount of ^{135}Cs can be produced in the Position-1 irradiation field adjacent to the core with a specially designed Test-assembly A for 1200 EFPD irradiation time. Consistent with the previous study, the neutron flux level in the outer reflector (Position-2) is not adequate considering a realistic irradiation time. The use of YH_2 moderator material inside the test-assembly A is found effective for the neutron spectrum adjustment. More importantly, we proved that the newly proposed gadolinia thermal neutron shielding adopted in test-assembly A can suppress the power peaks of the adjacent fuel assembly while maintaining a high transmutation rate of natural cesium into ^{135}Cs. Our study also shows that the reactivity of the insertion of the test-assembly A to the irradiation field adjacent

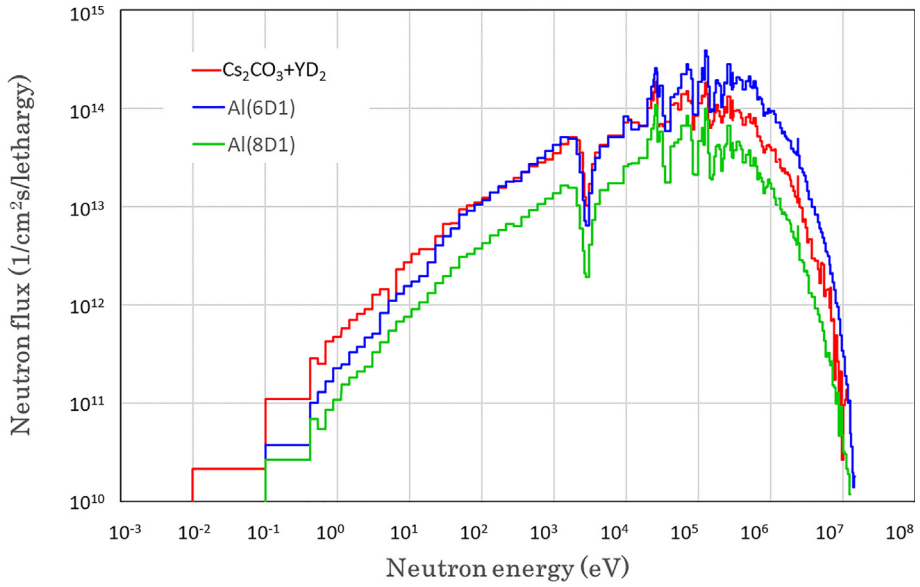

Fig. 21. Neutron spectra in the target pellets (Cs_2CO_3 + YD_2) of the test-assembly B and the surrounding moderators (Al).

Table 3
Summary of the production of ^{135}Cs.

Test-assembly(Loading position)	Moderator material	Target height	Number of targets*	Initial loading (^{133}Cs)	Production(^{135}Cs) Production rate**	
					360 EFPDs	1200 EFPDs
Assembly-A(Position-1)	YH_2	2 cm	1	152.8 mg	7.7 mg5.11 %/EFPY	36.0 mg7.17 %/EFPY
Assembly-B(Position-2)	YD_2	5 cm	37	14.14 g	12.6 mg0.09 %/EFPY	102.2 mg0.22 %/EFPY

* The target is the mixtures of Cs_2CO_3 and moderator, whose volume ratios are 5 % and 95 %, respectively.
** 1 EFPY = 365.25 EFPDs.

to the core can be compensated by the Joyo control rods. The results of our investigation and target subassembly design are expected to contribute to resolving the problem of providing a sufficient amount of ^{135}Cs for cross-section measurements to enhance the LLFP cross-section accuracy in the future.

CRediT authorship contribution statement

Yoshihisa Tahara: Investigation, Writing – original draft. **Peng Hong Liem:** Methodology, Software, Writing – review & editing. **Naoyuki Takaki:** Writing – review & editing. **Satoshi Chiba:** Supervision.

Declaration of Competing Interest

The authors declare that they have no known competing financial interests or personal relationships that could have appeared to influence the work reported in this paper.

Acknowledgments

The authors would like to thank Mr. H. Saito, Mr. W. Itagaki, and Dr. S. Maeda of Japan Atomic Energy Agency (JAEA) for helpful discussions and valuable suggestions on irradiation experiments using the Joyo experimental fast reactor and for preparing the data for nuclear calculations. We are grateful to Dr. Y. Tachi of JAEA for his advice and helpful comments on studying the irradiation experiment of LLFPs. This study includes the results of "Research and development of an innovative transmutation system of LLFP by fast reactors", entrusted to the Tokyo Institute of Technology by the Ministry of Education, Culture, Sports, Science and Technology of Japan (MEXT).

References

Aoyama, T. et al., 2005. Transmutation of Technetium in the Experimental Fast Reactor "JOYO". J. Nucl. Radiochem. Sci. 6 (3), 279–282.
Arie, K. et al., 2009. "A Strategy on Minimizing High-Level Waste Burdon for Sustainable Nuclear Energy System", Proceedings of Global 2009. France, Paper, Paris, p. 9087.
Chiba, S., Wakabayashi, T., Tachi, Y., Takaki, N., Terashima, A., Okumura, S., Yoshida, T., 2017. "Method to Reduce Long-Lived Fission Products by Nuclear Transmutations with Fast Spectrum Reactors. Sci. Rep. 7 (1). https://doi.org/10.1038/s41598-017-14319-7.
Fleming M. et al. (2018). "The Fispact-II User Manual," UKAEA-R(18)001.
IAEA (1982). "Evaluation of Actinide Partitioning and Transmutation," Technical Report Series No. 214, Vienna, Austria.
Itagaki, W. et al., 2017. "Measures to Meet New Regulations for Restart and the Irradiation Capability of Joyo", 5th International Workshop on Structural Materials for Innovative Nuclear Systems (SMINS-5). Kyoto, Japan.
Ikegami T. et al. (2001). "Study of Core Characteristics on Fuel and Coolant Type – Results of F/S Phase-I –, " JNC TY9400 2001-011.
JAEA (2021). Nuclear Data Center, Japan Atomic Energy Agency. URL: https://wwwndc.jaea.go.jp/jendl/jendl.html (Accessed date: August 10, 2021)
Kitano, A. et al., 2003. "MA/LLFP Transmutation Experiment Options in the Future Monju Core", GENES4/ANP2003. Kyoto, Japan, Paper, p. 1102.
LANL (2017). "MCNP® USER'S MANUAL Code Version 6.2," Los Alamos National Laboratory report LA-UR-17-29981.
Maeda, Y. et al., 2005. Distinguished achievements of a quarter-century operation and a promising project named MK-III in JOYO. Nucl. Technol. 150 (1), 16–36.
Maeda S. et al. (2014). "Characterization of Irradiation Fields for Fuel and Material Irradiation in the Experimental Fast Reactor JOYO," PHYSOR 2014 – The role of Reactor Physics Toward a Sustainable Future, The Westin Miyako, Japan, September 28-October 3, (2014).
Naganuma M. et al. (2006). "Study on Transmutation Technology of Long-Lived-Fission-Products (LLFP) Using Commercial Fast Reactors — Loading Type of LLFP

Target Assembly and Transmutation Performances of Cores Designed in FS Phase-II —," JAEA-Research 2006-063.
Nagaoki, Y., 2020. Current Status of Monju Decommissioning. IAEA Consultancy Meeting on Fast Breeder Reactors Decommissioning, Vienna, Austria.
NUMO (2018). "Nuclear Waste Management Organization of Japan, NUMO safety case report - Development of Pre-siting SDM-based Safety Case - (Draft for external review), Summary," NUMO-TR-18-02 (in Japanese).
NUMO (2018). "Nuclear Waste Management Organization of Japan, NUMO safety case report - Development of Pre-siting SDM-based Safety Case - (Draft for external review)," NUMO-TR-18-03 (in Japanese).
Sekimoto, H. et al., 1998. Trade-off between Neutron Excess and Long-term Toxicity Production by Employing LLFP Incineration. Ann. Nucl. Energy 25 (11), 793–799.
Shcherbakov, O., Furutaka, K., Nakamura, S., Sakane, H., Kobayashi, K., Yamamoto, S., Hori, J.-I., Harada, H., 2005. Measurement of Neutron Capture Cross Section of ^{237}Np from 0.02 to 100 eV. J. Nucl. Sci. Technol. 42 (2), 135–144.
Shibata, K. et al., 2011. JENDL-4.0: A New Library for Nuclear Science and Engineering. J. Nucl. Sci. Technol. 48[1], 1–30.
Sublet Jean-Christophe C. et al. (2016). "The FISPACT-II User Manual," UKAEA-R (11) 11 Issue 8.
Takaki N. et al. (2002). "A study on LLFP Transmutation using Fast Reactor in the Feasibility Study on Commercialized Fast Reactor Cycle Systems, " JNC TN9400 2002-067.
Takaki N. et al. (2003). "LLFP Transmutation Performance in Sodium, Pb-Bi and He Cooled Fast Reactors," JNC TN9400 2003-054.
Takaki N. et al. (2004). "LLFP Transmutation Performance in Sodium, Pb-Bi and He Cooled Fast Reactors-II," JNC TN9400 2004-028.
Wakabayashi, T. et al., 2019a. Core concept of simultaneous transmutation of six LLFP nuclides using a fast reactor. Nucl. Eng. Des. 352, 110208.
Wakabayashi, T., Tachi, Y., Takahashi, M., Chiba, S., Takaki, N., 2019b. Study on method to achieve high transmutation of LLFP using fast reactor. Sci. Rep. 9 (1). https://doi.org/10.1038/s41598-019-55489-w.
Wakabayashi, T. et al., 2020. A fast reactor transmutation system for 6 LLFP nuclides. Nucl. Eng. Des. 363, 110667.
Yang, W.S. et al., 2004. Long-Lived Fission Product Transmutation Studies. Nucl. Sci. Eng. 146, 291–318.
Yamano N. et al. (2021). "Estimation of uncertainty in transmutation rates of LLFPs in a fast reactor transmutation system via an estimation of the cross-section covariances," J. Nucl. Sci. Technol. 2021; 58(5): 567-578.